Stem Cell Reports
Article

ISSCR

OPEN ACCESS

BMP4-SMAD1/5/9-RUNX2 pathway activation inhibits neurogenesis and oligodendrogenesis in Alzheimer's patients' iPSCs in senescence-related conditions

Daiki Nakatsu,[1,8] Rina Kunishige,[1,2,8] Yuki Taguchi,[1,2] Naeko Shinozaki-Narikawa,[1] Kishiko Osaka,[1] Kayo Yokomizo,[1] Mami Ishida,[1] Shunsuke Takei,[3] Shoko Yamasaki,[4] Keita Hagiya,[5] Kotaro Hattori,[6] Tadashi Tsukamoto,[7] Masayuki Murata,[1,2] and Fumi Kano[1,*]

[1]Cell Biology Center, Institute of Innovative Research, Tokyo Institute of Technology, 4259 Nagatsuta, Midori-ku, Yokohama, Kanagawa 226-8503, Japan
[2]Multimodal Cell Analysis Collaborative Research Cluster, Tokyo Institute of Technology, 4259 Nagatsuta, Midori-ku, Yokohama, Kanagawa 226-8503, Japan
[3]System Development Department, Technology Solutions Sector, Healthcare Business Unit, Nikon Corporation, 471, Nagaodai-cho, Sakae-ku, Yokohama, Kanagawa 244-8533, Japan
[4]Mathematical Sciences Research Laboratory, Research & Development Division, Nikon Corporation, 471, Nagaodai-cho, Sakae-ku, Yokohama, Kanagawa 244-8533, Japan
[5]Fujifilm Corporation, 7-3 Akasaka 9, Minato-ku, Tokyo 107-0052, Japan
[6]Department of Bioresources, Medical Genome Center, National Center of Neurology and Psychiatry, 4-1-1, Ogawahigashi-cho, Kodaira, Tokyo 187-8551, Japan
[7]Department of Neurology, National Center Hospital, National Center of Neurology and Psychiatry, 4-1-1, Ogawahigashi-cho, Kodaira, Tokyo 187-8551, Japan
[8]These authors contributed equally
*Correspondence: kano.f.aa@m.titech.ac.jp
https://doi.org/10.1016/j.stemcr.2023.01.004

SUMMARY

In addition to increasing β-amyloid plaque deposition and tau tangle formation, inhibition of neurogenesis has recently been observed in Alzheimer's disease (AD). This study generated a cellular model that recapitulated neurogenesis defects observed in patients with AD, using induced pluripotent stem cell lines derived from sporadic and familial AD (AD iPSCs). AD iPSCs exhibited impaired neuron and oligodendrocyte generation when expression of several senescence markers was induced. Compound screening using these cellular models identified three drugs able to restore neurogenesis, and extensive morphological quantification revealed cell-line- and drug-type-dependent neuronal generation. We also found involvement of elevated Sma- and Mad-related protein 1/5/9 (SMAD1/5/9) phosphorylation and greater Runt-related transcription factor 2 (RUNX2) expression in neurogenesis defects in AD. Moreover, BMP4 was elevated in AD iPSC medium during neural differentiation and cerebrospinal fluid of patients with AD, suggesting a BMP4-SMAD1/5/9-RUNX2 signaling pathway contribution to neurogenesis defects in AD under senescence-related conditions.

INTRODUCTION

Alzheimer's disease (AD) is the most prevalent neurodegenerative disorder, and its global incidence is expected to increase further because of accelerated societal aging (Alzheimer's Association, 2020). The major clinical symptoms of AD, such as cognitive decline and olfactory impairment, are closely associated with neuronal cell loss in the hippocampus and olfactory bulb (Alzheimer's Association, 2020; Chen and Mobley, 2019; Dan et al., 2021; Zhang et al., 2016), in part because of neuronal cell death induced by β-amyloid (Aβ) plaque deposition and neurofibrillary tangle (NT) formation (Rajmohan and Reddy, 2017; Vyas et al., 2020). Thus, drugs that suppress Aβ plaque deposition and tau tangle formation, such as sodium oligomannate (also called GV-971) and aducanumab, are being developed to reduce the cognitive decline in AD (Cummings et al., 2019).

Besides Aβ- or tau-mediated neuronal cell death, inhibition of neurogenesis (NG) in the hippocampus and olfactory bulb is also being focused on because it is associated with olfactory and cognitive decline in AD (Fricker et al., 2018; Dard et al., 2019; Attems et al., 2014; Dan et al., 2021; Zhang et al., 2016). NG defects have been demonstrated previously in AD model mice, such as triple transgenic (3 × TG) mice, TG2576 mice, and APPswe/PS1ΔE9 mice (Hollands et al., 2017; Wirths, 2017). Furthermore, an increase in NG via overexpression of a neural transcription factor, NEUROD1, restores cognitive deficits in APP × PS1 mice (Richetin et al., 2015), indicating the possibility that NG restoration is a therapeutic approach for AD.

NG in the hippocampus is reported to continue even in human individuals of old age (Boldrini et al., 2018). Postmortem analysis of the AD brain revealed a decreased number of NG-marker-positive cells in the hippocampus among patients with AD at higher Braak stage (Malek-Ahmadi et al., 2018; Moreno-Jiménez et al., 2019). Additionally, Tobin et al. (2019) reported that neuroblast numbers are reduced in individuals with cognitive impairment compared with healthy controls. In contrast to the intensive clinical trials and studies around Aβ deposition and tau tangle formation, few have targeted NG for AD treatment, so it is still unclear whether enhanced NG can

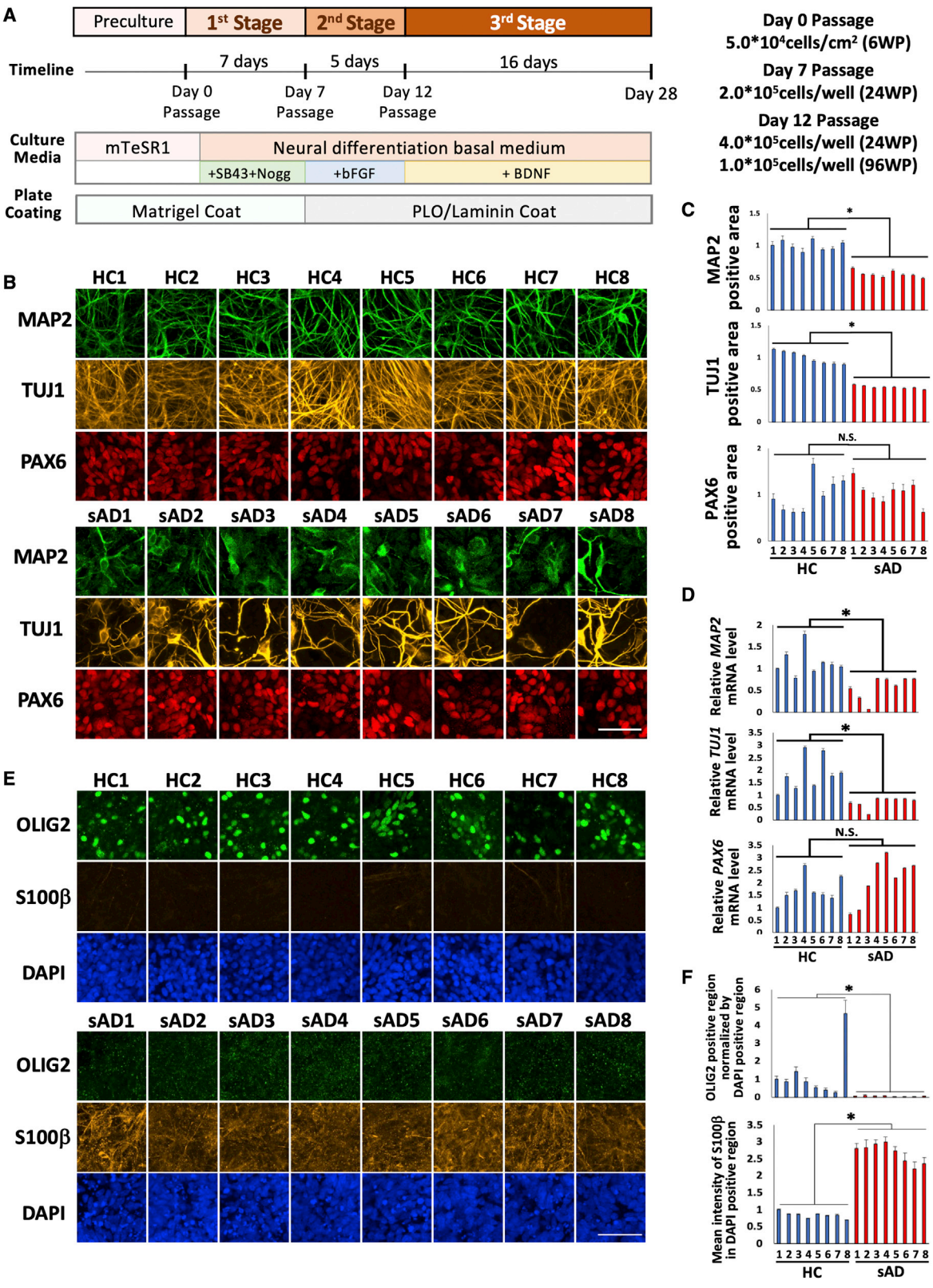

(legend on next page)

induce recovery of cognitive function (Cummings et al., 2019). Furthermore, the mechanisms underlying NG insufficiency in AD remain unexplored because of the inherent difficulties in evaluating NG in patients with AD.

Disease-specific induced pluripotent stem cells (iPSCs) are promising model systems for revealing the molecular mechanisms of the disease and as a platform for drug screening. Given that iPSC induction acts as a developmental reset, modeling age-related diseases such as sporadic AD (sAD) was thought to be difficult using iPSC-based systems. However, several recent studies have successfully recapitulated some core phenotypes of age-related diseases (Kondo et al., 2017; Nicaise et al., 2020), which may be explained by polygenic influences or epigenetic markers not eliminated by reprogramming. With AD, researchers created a model cell system that mimicked Aβ or tau abnormalities (Arber et al., 2021; Schulz, 2021). The iPSC-based drug screening mainly proposed novel candidate drugs for relieving Aβ deposition or neuronal cell death (Kondo et al., 2017; Pasteuning-Vuhman et al., 2021). In the current study, we developed a cellular model that recapitulated the NG defects in AD using familial AD (fAD) and sAD patient-derived iPSCs. During neural induction culture, these iPSCs exhibited impaired generation of neurons and oligodendrocytes but enhanced differentiation into astrocytes only when expression of several senescence markers was introduced by a low-density culture protocol. This deficit was associated with BMP4 hypersecretion and ensuing activation of Sma- and Mad-related protein 1/5/9 (SMAD1/5/9)-Runt-related transcription factor 2 (RUNX2) signaling, whereas inhibition of this signaling pathway rescued NG. Finally, we present evidence suggesting BMP4 hypersecretion in patients with AD.

RESULTS

The impaired generation of neurons was reconstituted in sAD and fAD iPSCs

We used 18 iPSC lines generated from 8 unrelated healthy control (HC) individuals, 8 unrelated patients with sAD, and 2 patients with fAD (Table S1). We first examined the undifferentiated state and the three-germ-layer differentiation potential of HC and AD iPSC lines. Immunofluorescence and quantitative real-time PCR analysis revealed that OCT4, Nanog Homeobox (NANOG), *TRA1-60*, and *miRNA371-3*, which are markers of the undifferentiated state in iPSCs, were significantly expressed in HC and AD iPSC lines (Figures S1A–S1E). We also confirmed that these cell lines could differentiate into endoderm, ectoderm, and mesoderm (Figure S1F). Next, we analyzed the neuronal differentiation of HC and AD iPSC lines. First, we adopted a modified version of the 3-stage neural differentiation method described by Wattanapanitch et al. (2014), which successively induces neural stem cells (NSCs) and neurons over 28 days (Figure 1A). When cells were seeded at a density of 5×10^4 cells/cm^2 on day 0, neurons and NSCs were generated from HC iPSC lines on day 28, as shown by immunofluorescence using antibodies against MAP2, a marker of mature neurons; TUJ1, a marker of immature neurons; and PAX6, a marker of NSCs (Figure 1B). However, we observed NG defects in 8 sAD and 2 fAD iPSCs via immunofluorescence as well as quantitative real-time PCR analysis (Figures 1B–1D, S2A, and S2B). We also performed analysis of the immunofluorescence images of MAP2, TUJ1, and PAX6, an NSC marker, of 8 HC and 8 sAD cells (Figure 1B). We measured the area of MAP2-, TUJ1-, or PAX6-positive cells, and the quantitated data supported inhibited formation of TUJ1- and MAP2-positive neurons but not PAX6-positive NSCs in AD (Figure 1C). The variation in NG across cell lines was also shown (Figure 1C). We investigated the time course for the protein and mRNA expression of *MAP2*, *TUJ1*, and *PAX6* at 0, 5, 10, 15, 20, 25, and 28 days after neuronal differentiation in HC1, an HC iPSC line, and sAD3, an sAD iPSC line, via western blot and quantitative real-time PCR, respectively (Figures S3A–S3G). The results indicated that the deficiency in neuronal generation of sAD3 was not due to repressed differentiation into NSCs but repression of NSC differentiation into neurons.

To investigate whether these observed NG abnormalities were associated with alterations in differentiation fate, we examined expression levels of the oligodendrocyte markers oligodendrocyte transcription factor 2 (OLIG2) and myelin basic protein (MBP) as well as the astrocyte markers S100

Figure 1. Neuronal, oligodendrocyte, and astrocyte differentiation potentials of iPSCs from HCs and patients with sAD under low-density culture conditions

(A) Schematic of neuronal differentiation of iPSCs under low-density culture conditions. Control (HC1–HC8) and sAD (sAD1–sAD8) iPSCs were analyzed on day 28.

(B and C) Immunofluorescence of MAP2, TUJ1, and PAX6. Mean positive area was quantified in (C) Scale bar, 50 μm. *$p < 0.05$, n = 13 images taken from the same well per group.

(D) Quantitative real-time PCR analysis of *MAP2*, *TUJ1*, and *PAX6* mRNA expression. Mean mRNA levels in HC1 were set to 1. n = 4–6 independent experiments. *$p < 0.05$.

(E and F) Immunofluorescence and quantification of OLIG2 and S100β. *$p < 0.05$, n = 15 images taken from the same well per group. Scale bar, 50 μm.

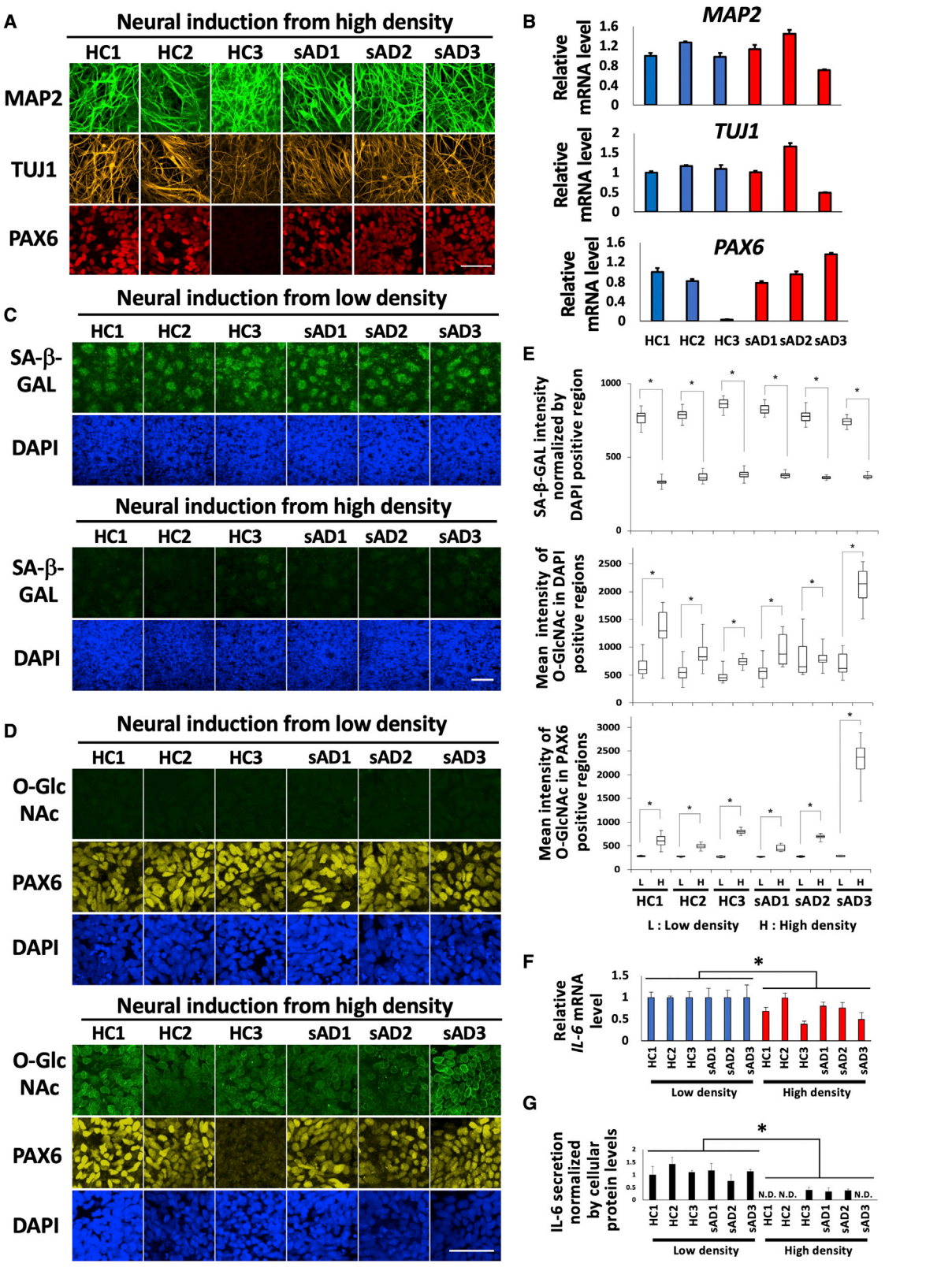

(legend on next page)

β-subunit (S100β) and vimentin (VIM) via western blot and immunofluorescence on day 28 after neural induction. Immunofluorescence demonstrated that OLIG2-positive cells differentiated routinely from HC cells but rarely from sAD-derived cells (Figures 1E and 1F). In contrast, broad expression of S100β among all sAD-derived cells was observed, which may be caused by the premature state of astrocyte differentiation. However, it is noteworthy that we found no significant expression (fluorescence signal) of S100β from HC-derived cells (Figure 1E). Western blot analysis also supported the results of immunofluorescence (Figure S1G). These results indicated less oligodendrocyte generation and increased differentiation toward astrocytes in AD iPSCs.

To ensure that the NG abnormalities observed in AD-derived cell lines were not due to excessive cell death, we conducted immunofluorescence analysis using antibodies against the apoptotic cell marker cleaved caspase-3 (cCASP3) and cell viability analysis using trypan blue. Surprisingly, the number of cCASP3-positive dead cells was actually greater in cultures of HC iPSCs than in cultures of AD iPSCs (Figures S1H, S2C, S3D, and S3H), likely reflecting the known death of many newborn neurons generated from NSCs before maturity (Toda et al., 2019). These results indicate that neural cell death was not the cause of decreased NG in AD cells.

Next, we focused on Aβ40 and Aβ42 because Aβ is a possible regulator of NG defects (Li Puma et al., 2019; Scopa et al., 2020). ELISA confirmed no significant increase in extracellular secretion of Aβ40 and Aβ42 and the secretion rate of Aβ42/Aβ40 from sAD iPSCs compared with healthy iPSCs (Figures S3I–S3K). However, we observed that the Aβ oligomer level substantially increased in 3 sAD cells compared with 3 HC cells (Figure S3L). These results suggest that the inhibition of neural differentiation might be attributed to increased Aβ oligomers.

An AD-specific NG defect was observed when expression of several senescence markers was induced by low-density seeding of iPSCs

Individuals ultimately developing AD show normal brain development and structure, including normal whole-brain and hippocampal size, until middle age (Coupé et al., 2019). Because repression of NG occurs in elderly patients with AD (Moreno-Jiménez et al., 2019; Tobin et al., 2019), we hypothesized that this protocol more likely recapitulates aged adult NG rather than embryonic NG. Furthermore, we found that the observed NG defect in sAD-derived iPSCs could be alleviated by a slightly modified protocol in which the cells were seeded at higher density (4×10^5 cells/cm^2) on day 0, whereas other conditions, including cell density during stages II and III, were maintained as in the initial "low-density" protocol (Figures 2A and 2B). When cells were seeded at high density, neurons were generated from all 3 HC and 3 sAD iPSC lines on day 28 (Figure 2A) with no significant difference in the number of dead cells (Figure S4A). Also, there was no significant difference in cell number on day 28 between low- or high-density differentiation conditions (Figure S4B). These observations led us to examine whether the NG defects in AD cells observed using the low-density protocol were associated with senescence phenotypes.

To this end, we first compared expression of the well-known senescence marker senescence-associated β-galactosidase (SA-β-gal) (He et al., 2013) on day 28 between three HC-derived iPSC lines (HC1–HC3) and three sAD-derived iPSC lines (sAD1–sAD3), which are similar in tissue origin and iPSC transgene expression (Table S1), under high- and low-density culture conditions. Interestingly, the SA-β-gal signal was observed only under low-density differentiation conditions in the radially organized cell structure (Figures 2C and 2E). N-cadherin (NCAD) was shown to be polarized at the center of this structure (Figure S4C), which indicated that this structure was the pluripotent neural precursor cell rosettes observed during early neural tube formation (Zhang et al., 2001; Elkabetz et al., 2008). We then confirmed that these neural rosette-like structures were formed to the same extent by HC- and sAD-derived cells under high- and low-density protocols (Figure S4C). Thus, the low-density protocol increased the signal of SA-β-gal within neural rosettes in HC- and AD-derived cultures but did not change the efficiency of neural rosette formation.

We also examined the expression level of cellular senescence markers by immunofluorescence staining for O-linked-β-*N*-acetylglucosamine (O-GlcNAc) and nuclear

Figure 2. Senescence-related propensities of HC and sAD cells under low- and high-density culture conditions

Control (HC1–HC3) and sAD (sAD1–sAD3) iPSCs were analyzed after neuronal differentiation for 28 days.

(A and B) Neuronal differentiation potential under high-density culture conditions was analyzed by immunofluorescence (A) and quantitative real-time PCR analysis (B) of MAP2, TUJ1, and PAX6 (n = 4 independent experiments).

(C–E) Immunofluorescence of SA-β-gal (C) and O-GlcNAc (D) on day 28 under low- or high-density culture conditions, quantified in (E). n = 10–15 images taken from the same well per group.

(F and G) The mRNA levels of IL-6 were quantified by quantitative real-time PCR analysis (F), and the IL-6 protein levels in the medium were quantified by ELISA (G).

Mean mRNA or protein levels in HC1 were set to 1. *p < 0.05. n = 4–6 independent experiments. Scale bars, 50 μm.

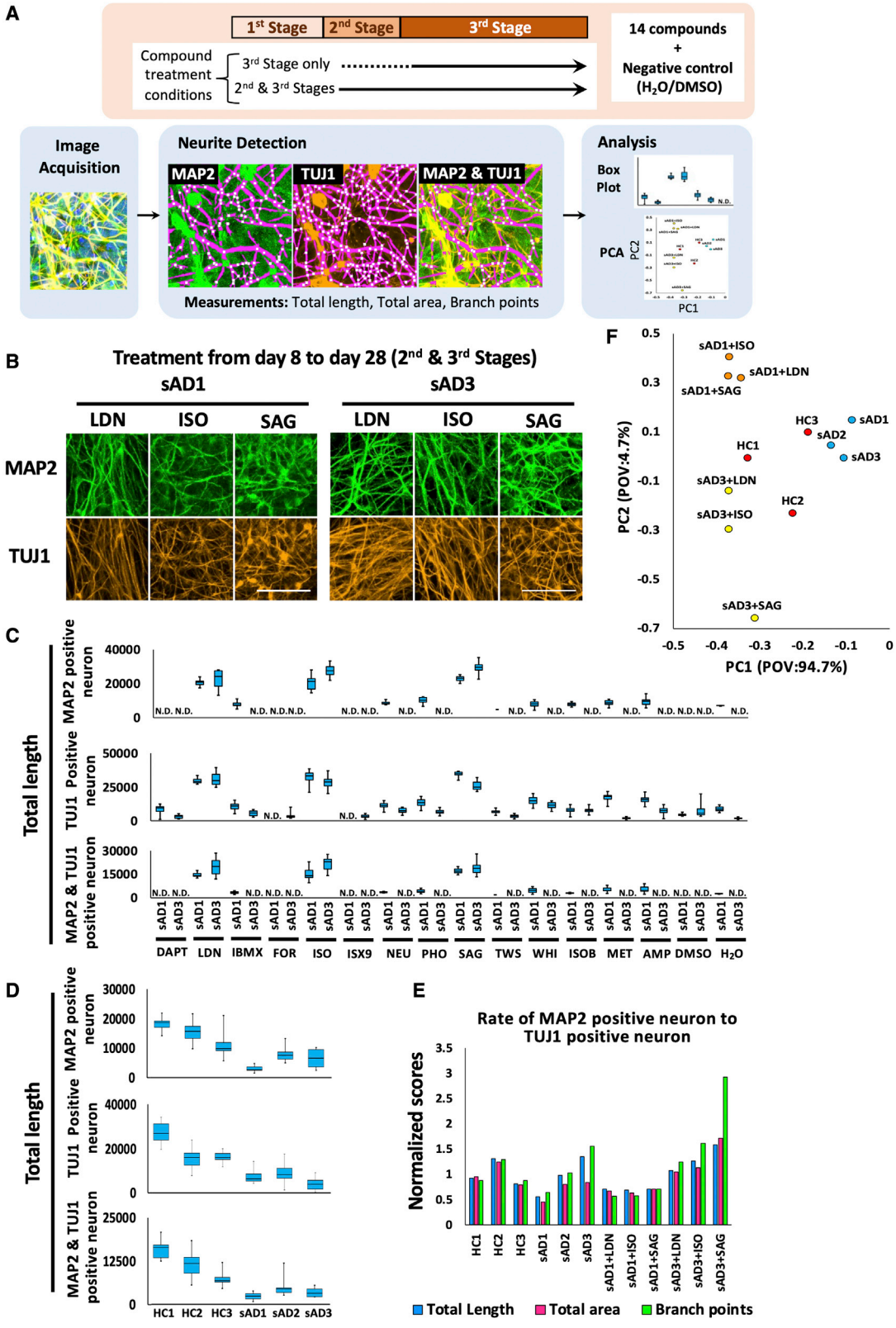

(legend on next page)

factor-erythroid 2-related factor 2 (NRF2). O-GlcNAcylation of proteins is known to be reduced in aged mice, and this loss was associated with impairment of learning and memory (Wheatley et al., 2019). In addition, decreased expression of NRF2, a transcription factor that regulates the various stress responses, has been reported previously in hippocampal NSCs of aged mice (Ray et al., 2018). The O-GlcNAc signal was observed mainly in the nucleus of PAX6-positive HC and AD cells under the high-density culture condition (Figures 2D and 2E), whereas NRF2 was diffusely localized to the nucleus and the cytoplasm (Figures S4D and S4E). Both signals were not limited to the neural rosette but observed among most cells and reduced in low-density culture (Figures 2D and S4D). Moreover, expression and secretion of interleukin-6 (IL-6), a proinflammatory cytokine upregulated during senescence (referred to as a senescence-associated secretory phenotype [SASP]; Nicaise et al., 2020), was greater in low-density cultures of HC- and AD-derived iPSCs than in corresponding high-density cultures (Figures 2F and 2G). These results suggested that the low-density protocol induced the cell senescence-related state, especially in NSCs forming neural rosettes, indicating the possibility that our neural differentiation system might recapitulate the NG defect of elderly patients with AD.

Image-based screening of small chemical compounds for improving NG in AD iPSCs

We next used these AD-derived iPSCs demonstrating abnormal NG under senescence marker expression conditions by the low-density protocol to screen for compounds that can increase NG. Therefore, we chose 14 small chemical compounds reported to enhance NG whose concentration was determined by previous studies (Table S2). Two AD iPSC lines, sAD1 and sAD3, were used for screening. sAD2 could not be used because dimethyl sulfoxide (DMSO) treatments caused cell death. The compounds and vehicle (either water or DMSO) were added to cultures from days 8–28 (stages II and III) or from days 13–28 (stage III only) (Figure 3A). We chose 0.66% DMSO and 0.5% H_2O as negative controls to match the highest concentrations of DMSO and H_2O contained in the reagents. Changes in NG were examined by immunofluorescence staining for TUJ1 and MAP2. Although no compound restored NG when applied only during stage III (Figure S5A), three compounds increased NG in both AD-derived iPSC lines when applied during stages II and III (Figure S5B): LDN-193189 (LDN), smoothened agonist (SAG), and isotretinoin (ISO). These results indicate that the NSC induction stage (stage II) is a crucial time window for modulating neural differentiation potency.

LDN is an inhibitor of the bone morphogenetic protein (BMP) type I receptors activin receptor-like kinase-2 (ALK2) and ALK3 (Yu et al., 2008), whereas ISO is an activator of retinoic acid receptors, and SAG is an activator of Smoothened (Chen et al., 2002; Lane and Bailey, 2005). The neurons created by each compound appeared distinct in structure, especially after SAG treatment (Figure 3B). Therefore, an image-based morphological analysis was performed to detect compound-specific differences in neuronal generation (Figure 3A). First, the TUJ1- or MAP2-positive area was segmented to enable specific measurement of cell dimensions and the number of branchpoints per frame (detailed in Figures S5C and S5D and supplemental experimental procedures). Although nonspecific staining of MAP2 was sometimes observed in the nucleus and cytoplasm of apparently non-neuronal cells, these signals could be excluded during image analysis, enabling precise quantification of neurites. Measuring these values as feature quantities enabled quantitative comparisons of drugs and cell lines (Figures 3C–3F, S5E, and S5F). For example, more neurons were generated from HC1 than from HC3 (Figures 3D, S5E, and S5F). In addition, the maturation status of generated neurons was higher in sAD3 following SAG treatment than LDN or ISO treatment, as indicated by the MAP2/TUJ1 ratio (Figure 3E).

Subsequently, we performed principal-component analysis (PCA) using quantified data of the images taken on day 28 of HC1-3, sAD1-3, and sAD1 or sAD3 treated with the 3 drugs (Figure 3F). PC1 or PC2 may be related to features of neuronal generation (e.g., length, area, and branchpoints) or of the immature state of the neurons (e.g., the ratio of TUJ1-positive neurons to MAP2-positive neurons) (Table S3). This analysis showed that the cell lines that created neurons could be separated from those that

Figure 3. Image-based screening of small chemical compounds for improving NG of sAD iPSCs

(A) Outline of the compound screening experiments. Cells were treated with the compounds during stages II and III or only during stage III. Cells were fixed on day 28, followed by immunofluorescence and image analysis to detect MAP2- and/or TUJ1-positive neurites (detailed in Figure S5).

(B) Representative images of MAP2 and TUJ1 staining in LDN-, ISO-, and SAG-treated sAD1 and sAD3 cells (excerpt from Figure S5B). Scale bars, 50 μm.

(C and D) Total length of MAP2- and/or TUJ1-positive neurites. n = 10–15 images taken from the same well per group.

(E) Ratio of the total length, total area, and branchpoints of MAP2-positive neurons to TUJ1-positive neurons.

(F) PCA using morphological features (total length, total area, and number of branchpoints).

could not along the PC1 axis (Figure 3F). Interestingly, we observed AD cell line-specific clusters when the cells were treated with 3 drugs; sAD1 treated with the 3 drugs appeared in the upper left, whereas sAD3 treated with the 3 drugs was in the lower left area (Figure 3F). This indicates the possibility that characteristics of each cell line affected neuronal features generated by drug treatment, which were visualized using image-based quantification coupled with PCA. Because sAD3 treated with LDN was the closest to HC1 in the PCA plot, we examined how LDN contributes to restoring neuronal generation in sAD3.

LDN treatment during NSC differentiation was crucial for improving neural generation in AD iPSCs

We next analyzed the duration of LDN treatment and found that treatment during stage II (i.e., differentiation to NSCs), was sufficient to induce generation of neurons in sAD3. Immunofluorescence and quantitative real-time PCR analysis of sAD cells revealed that MAP2- and TUJ1-positive neurons were created even when LDN was added during days 8–12 to the same extent as when LDN was added from days 8–28 (Figures 4 and S6A). This was also true in fAD iPSCs (Figures S2D–S2G). This indicated that the potential for differentiation into neurons was strongly affected or changed during neuronal stem cell differentiation and was enhanced via treatment with LDN during stage II. Subsequently, we examined whether NSC marker expression differed between HC and AD cells. The expression levels of the NSC markers were examined in HC and AD cells on the final days of stages II and III by immunofluorescence using antibodies against PAX6, NESTIN, and SOX1 (Figures 2D, S6B, and S6C). Quantification of occupying areas or fluorescence signals of these markers showed no substantial difference between HC and sAD cells (Figures S6B–S6D).

LDN is known to repress activation of SMAD1/5/9 (Yu et al., 2008), a protein known to be activated in AD model SAMP8 mice and APPswe/PS1(DeltaE9) transgenic mice (Tang et al., 2009; Díaz-Moreno et al., 2018). Thus, we hypothesized that SMAD1/5/9 activation by phosphorylation may contribute to the NG defect in AD iPSCs. We immunostained phosphorylated SMAD1/5/9 (P-SMAD1/5/9) on the final day of neural differentiation (day 28) in 8 HC, 8 sAD, and 2 fAD cells and found that phosphorylation of SMAD1/5/9 was clearly increased in sAD and fAD iPSCs (Figures 5A–5C, S2H, and S2I). This was repressed by treatment with LDN during stage II (Figures 5A, S2H, and S2I). Moreover, LDN treatment of AD iPSCs during stage II restored the defect in oligodendrocyte formation and reduced expression of the astrocyte marker S100β, as shown by immunofluorescence (Figures 5D, S2H, and S2I). These results strongly suggest that the increased phosphorylation of SMAD1/5/9 during stage II inhibits generation of neurons and oligodendrocytes and, alternatively, enhances differentiation toward astrocytes in AD iPSCs.

RUNX2 expression in sAD and fAD iPSCs reduces generation of neurons and oligodendrocytes

We next focused on factors that change the potential for neuronal differentiation downstream of phosphorylated SMAD1/5/9. A candidate was RUNX2, which reportedly enhances the development and maturation of astrocytes from NSCs (Okawa et al., 2016; Tiwari et al., 2018). Also, single-cell RNA sequencing (RNA-seq) analysis of olfactory mucosal cells of AD patients revealed that transcriptional regulation by *RUNX2* was significantly increased in AD patients compared with HCs (Lampinen et al., 2022). Therefore, we examined the expression of *RUNX2* via quantitative real-time PCR during neuronal differentiation of 8 HC, 8 sAD, and 2 LDN-treated sAD cells and 2 fAD cells with or without LDN treatment. This demonstrated that *RUNX2* was more highly expressed in AD cells than in HC cells, which was inhibited by LDN treatment (Figures 6A and 6B). To confirm the involvement of RUNX2 in inhibition of NG in AD iPSCs, neural induction of sAD and fAD iPSCs was performed in the presence of CADD522, an inhibitor of RUNX2-dependent transcriptional activation by inhibiting the binding of RUNX2 to DNA. CADD522 or DMSO was applied on days 15–28 because *RUNX2* expression was elevated from day 15 (Figure 6A). Immunofluorescence and quantitative real-time PCR analysis demonstrated that CADD522 treatment increased the number of MAP2- and TUJ1-positive neurons along with an increase in the mRNA expression levels of *TUJ1* and *MAP2* (Figures 6C and 6D). Moreover, differentiation into astrocytes decreased, whereas differentiation into oligodendrocytes and the number of cCASP3-positive cells increased by CADD522 treatment in sAD and fAD iPSCs (Figures 6E and 6F), which was consistent with the results seen after LDN treatment. These results suggest that *RUNX2* expression downstream of SMAD1/5/9 is a key factor that represses generation of neurons and oligodendrocytes while enhancing differentiation into astrocytes in AD iPSCs. Next, to elucidate the connection between our cellular model findings and *in vivo* data, P-Smad1/5/9 and Runx2 expression levels were measured in the hippocampus of SAMP8, a senescence-accelerated sAD model mouse (Díaz-Moreno et al., 2018). We observed an increased protein level of phosphorylated Smad1/5/9 and Runx2 in SAMP8 compared with SAMR1, a control mouse (Figure 6G).

Elevated BMP4 level in medium of AD cells and in cerebrospinal fluid samples from patients with AD

We next examined upstream factors that activate phosphorylation of SMAD1/5/9. Given that SMAD1/5/9 was

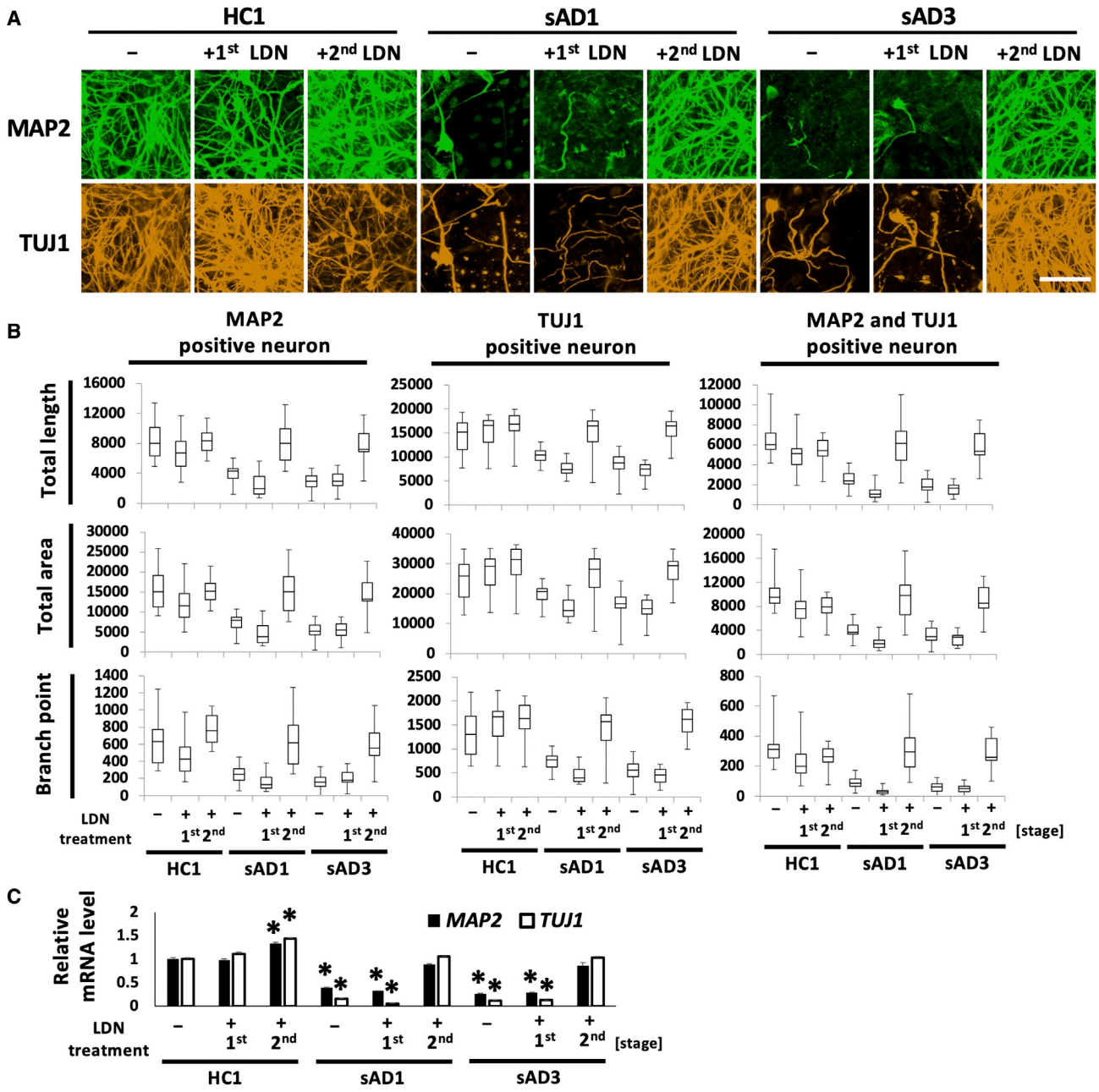

Figure 4. Effect of LDN on neural differentiation of HC and sAD iPSCs

Control (HC1) and sAD iPSCs (sAD1 and sAD3) were cultured under low-density conditions and treated with or without 250 nM LDN during stage I or stage II of neuronal differentiation (+first LDN or +second LDN, respectively).

(A) Immunofluorescence of MAP2 and TUJ1. Scale bar, 50 μm.

(B) Quantification of MAP2- and/or TUJ1-positive neurites in (A) (detailed in Figure S5). n = 15 images taken from the same well per group.

(C) Quantitative real-time PCR analysis of mRNA expression levels of *MAP2* and *TUJ1*. Mean mRNA levels in HC1 were set to 1. n = 4 independent experiments, *p < 0.05 compared with non-treated HC1 cells.

downstream of the BMP receptors, we focused on the BMP family. First, using quantitative real-time PCR, we measured the mRNA expression levels of *BMP2*, *BMP4*, *BMP5*, *BMP6*, *BMP7*, *BMP9*, and *BMP10* , BMP family members mainly involved in phosphorylation of SMAD1/5/9 (Sanchez-Duffhues et al., 2020), on day 28. The expression levels of *BMP4* and *BMP7* were specifically increased in three sAD- and two fAD-derived iPSC lines compared

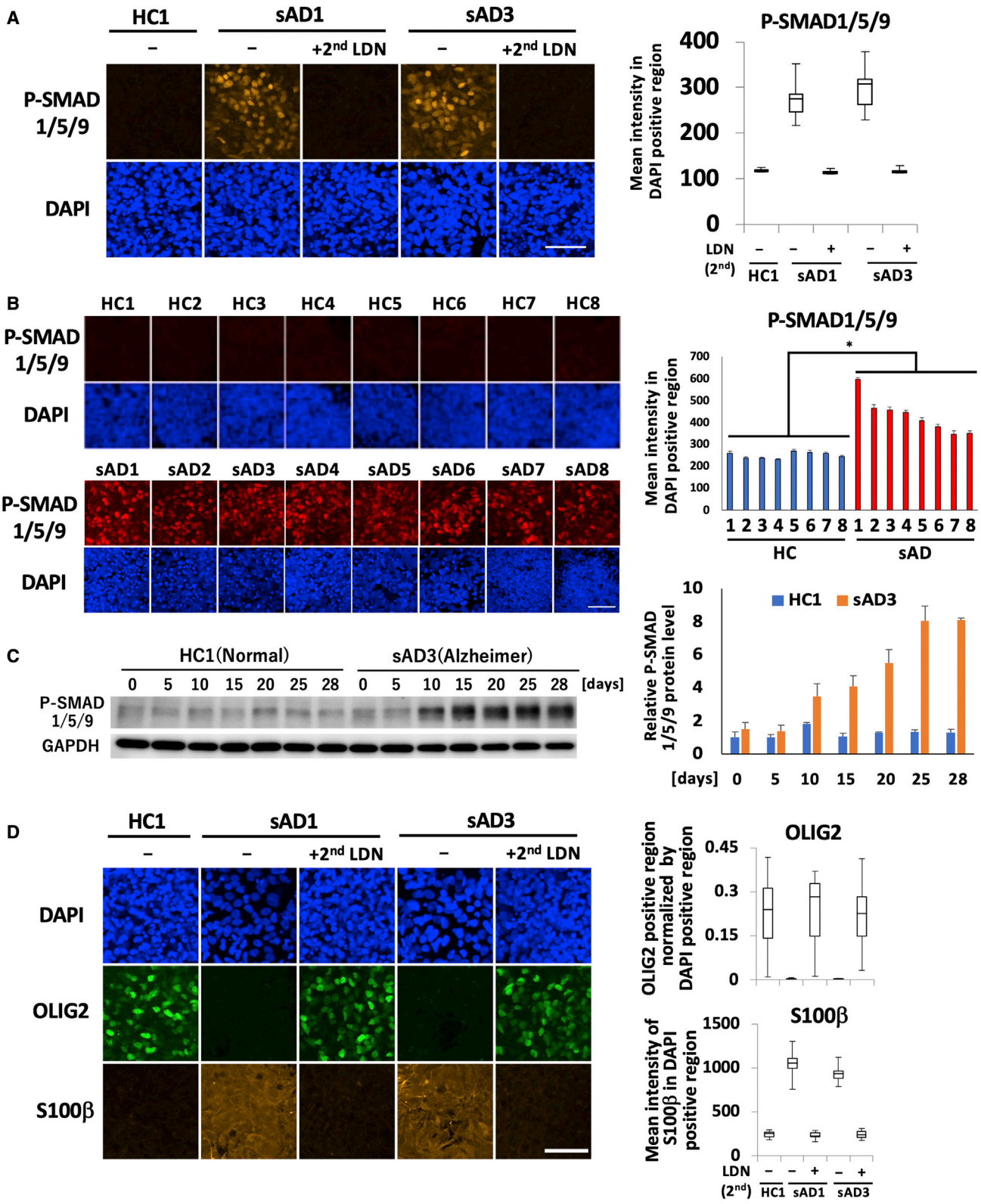

(legend on next page)

with four HC-derived lines (Figures 7A and 7B). In addition, ELISA revealed that BMP4 protein level was enhanced in the medium from sAD1, sAD3, fAD1, and fAD2 cultures, suggesting enhanced secretion, and this elevation was inhibited in all four lines by LDN treatment (Figure 7B). In contrast, no BMP7 protein was detected in the medium of any HC, sAD, or fAD line (Figure 7C). These results suggest that secreted BMP4 may contribute to the observed NG abnormality of AD-derived iPSCs by inducing excess phosphorylation (activation) of SMAD1/5/9.

qPCR results showed that *BMP4* expression increased in a time-dependent manner in AD iPSCs (Figure 7D). Because the AD-specific elevation in *BMP4* expression occurred on day 5 and that of phospho-SMAD1/5/9 and *RUNX2* on days 10 and 15, respectively (Figures 5C, 6A and 7D), enhanced BMP4 expression might trigger the change in the potency of neural differentiation at the early stage.

A possible cause of AD-specific BMP4 upregulation is epigenetic modification. Therefore, we tested the DNA methylation level, an epigenetic mark for gene repression, of 6 CpG sites in the *BMP4* promoter (Figure 7E). These sites were chosen because methylation analysis has been reported in these sites in healthy human iPSCs (Clough and Barrett, 2016). First, we performed a PCR-based analysis of the bisulfite-treated DNA genome of HC1 and sAD3, which showed a decrease in DNA methylation at site cg24526899 in sAD3 (Figure 7E). We further analyzed the DNA methylation level of cg24526899 through quantitative enzyme-based analysis of bisulfite-converted genome DNA prepared from 7 HC cells and 5 sAD cells. The results showed that the DNA methylation level of cg24526899 commonly decreased in AD cells (Figure 7F). Furthermore, treatment with a DNA methylation inhibitor, 5-aza-2′-deoycytidine, increased the *BMP4* expression level in HC iPSC even on day 0 (the undifferentiated condition) (Figure 7G). These results suggest that decreased methylation of the *BMP4* promoter upregulates BMP4 protein expression in AD cells.

Finally, to investigate the significance of BMP4 hypersecretion in AD pathology, we examined the amount of BMP4 in cerebrospinal fluid obtained from 20 HCs and 20 patients with AD by ELISA (Table S4). Interestingly, consistent with elevated secretion in AD iPSCs, BMP4 concentration was significantly higher in cerebrospinal fluid samples from patients with AD (Figure 7H). Collectively, these findings suggest that cerebrospinal fluid BMP4 may be an accessible biomarker for AD pathology.

DISCUSSION

In this study, we demonstrated that all 8 sAD-derived iPSCs and 2 fAD-derived iPSC lines exhibited deficient NG and oligodendrogenesis but enhanced differentiation toward astrocytes when expression of several cell senescence markers was induced (Figures 1, 2, S2A, and S2B). The cell density during stage I altered the expression of cell senescence markers by day 28 in HC-derived and AD-derived cultures. Expression of the senescence marker SA-β-gal was substantially elevated by the low-density seeding condition at neural rosettes (Figures 2C and S4C). Meanwhile, the decreased expression of O-GlcNAc as well as NRF2, another aging marker, was not limited to a specific cell type (Figures 2D and S4D). Considering that neural progenitor cells at neural rosettes have the ability to differentiate into neurons, oligodendrocytes, and astrocytes, we suppose that the senescence-associated phenomena in broad types of cells might be originating from the SA-β-gal-positive NSCs. Another possibility is the effect of paracrine factors secreted from SA-β-gal-positive NSCs. We found that one of the inflammatory paracrine factors, IL-6, was secreted more under the low-density seeding condition (Figure 2G). Interestingly, IL-6 treatment induced cell senescence (confirmed by SA-β-gal staining) in the breast cancer cell line MCF-7 (Ortiz-Montero et al., 2017). Additionally, IL-6 signaling has been reported to be necessary for the self-renewal and maintenance of NSCs (Storer et al., 2018), suggesting that IL-6 possibly affects the fate of NSCs.

The NG defect observed in this study was detected under a limited condition, when the expression of several senescence markers was induced by a low-density seeding protocol. In fact, sAD iPSCs normally developed neurons under high-density conditions when no senescence markers were observed in the cells. The question is how the status induced by the low-density seeding protocol is related to AD-cell-specific NG defects and AD pathology. To this

Figure 5. Increased phosphorylation of SMAD1/5/9 in sAD cells

(A) HC1, sAD1, and sAD3 cells were immunostained with phosphorylated SMAD1/5/9 antibody (P-SMAD1/5/9) after induction of neuronal differentiation for 28 days with or without 250 nM LDN treatment during stage II. n = 10–15 images taken from the same well per group. Scale bar, 50 μm.

(B) Immunofluorescence of P-SMAD1/5/9 in HC1-8 and sAD1-8 on day 28. Scale bar, 50 μm.

(C) Protein expression of P-SMAD1/5/9 in HC1 and sAD3 cells 0, 5, 10, 15, 20, 25, and 28 days after neuronal differentiation were analyzed by western blot. The mean protein levels on day 0 of HC1 were set to 1. n = 3 independent experiments.

(D) Immunofluorescence of OLIG2 and S100β and its quantification. Scale bar, 50 μm n = 10–15 images taken from the same well per group. *$p < 0.05$.

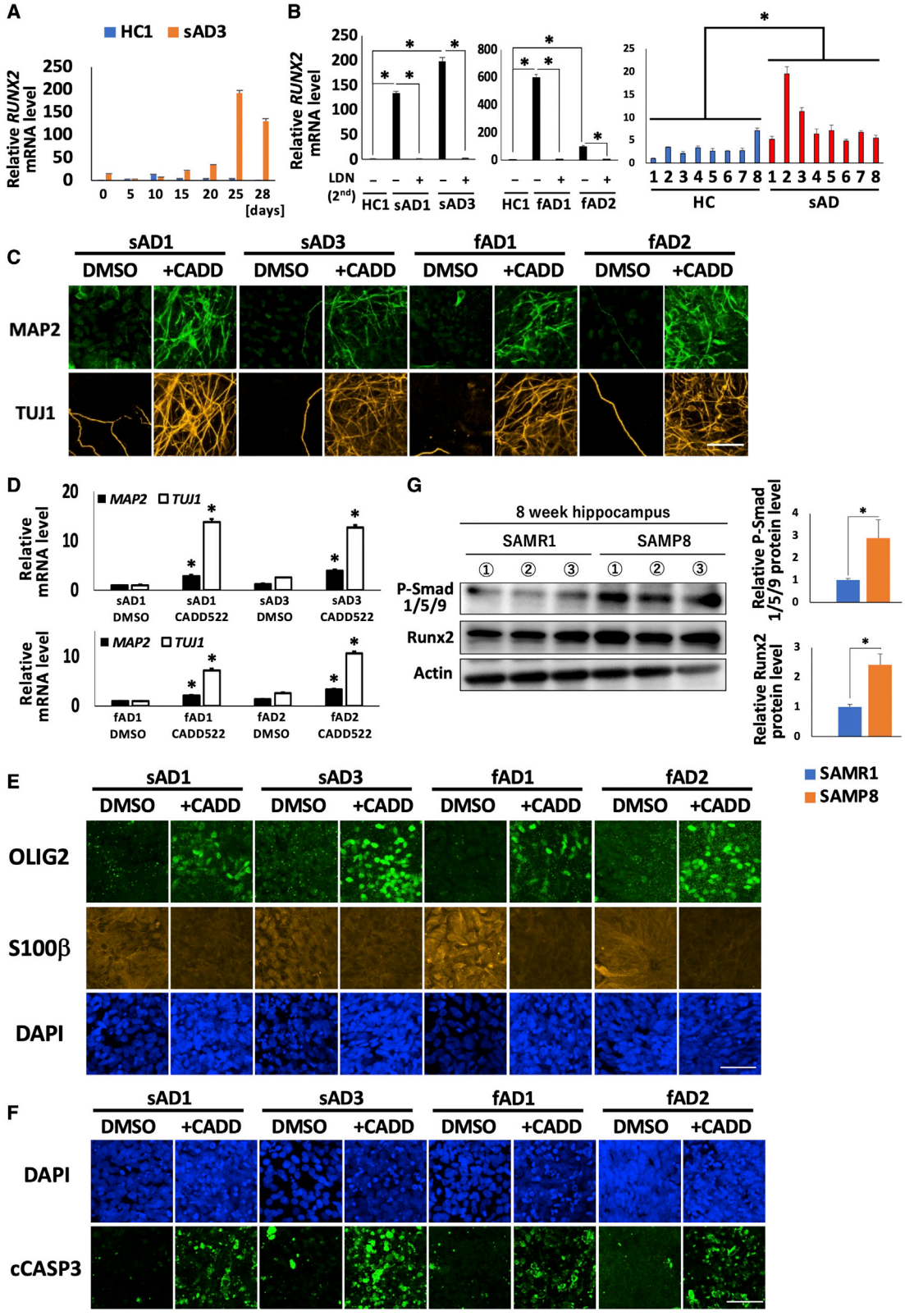

(legend on next page)

end, evaluation of our findings using other widely used AD models is necessary. Transgenic mouse models based on the genetic fAD mutations or *App* or *Psen* overexpression offer great insight into the molecular mechanisms of how Aβ deposition and NTs are formed and contribute to AD pathology. In addition, 3D cell systems, such as brain organoids, are powerful platforms to recapitulate disease phenotypes where aberrant processes are considered to depend on interaction between neurons and other cell types (Drummond and Wisniewski, 2017). Recently, Chen et al. (2021) succeeded in *in vitro* reconstitution of increased Aβ aggregates and phosphorylated tau protein using brain organoids. Because we found increased Aβ oligomer levels in AD cells (Figure S3L), there might be some link between the repressed NG in our study and the Aβ hypothesis, which should be evaluated using these well-established AD models in future studies.

How sAD iPSCs share a common phenotype remains a pivotal but unclarified issue in AD pathology. We propose at least three possibilities for this study. First, epigenetic modification patterns contribute to the AD-specific common phenotype. Interestingly, cg24526899, one of the six CpG sites in the *BMP4* promoter, showed an AD-cell-line-specific decline in methylation (Figures 7E and 7F). Furthermore, treatment with a DNA methylation inhibitor increased *BMP4* expression levels in HC iPSCs even on day 0, the undifferentiated condition (Figure 7G). These results suggest epigenetic differences in the *BMP4* promoter as a key regulator of the commonly repressed NG of AD iPSCs. Second, the common inhibition of NG in AD might result from differences in Aβ production, ratio, and quality, among other factors. We observed that the Aβ oligomer increased in 3 AD cells compared with 3 HC cells (Figure S3L), although there was no specific trend in production of Aβ40 and Aβ42 or the Aβ42/Aβ40 ratio (Figures S3I–S3K). These results are noteworthy because an increase in intracellular Aβ oligomers impairs olfactory bulb and adult hippocampal NG (Li Puma et al., 2019; Scopa et al., 2020), consistent with the toxic Aβ oligomer hypothesis (Cline et al., 2018). Third, a combination of polygenic variants is associated with AD pathology, which has been revealed by genetic analysis and genome-wide association studies (GWASs) (Cline et al., 2018; Kondo et al., 2022). Hence, we consider that such a combination of rare gene variants might result in the shared phenotype in sAD cells. We also propose that, although the common phenotypes of sAD iPSCs could originate from such combined factors, further research is warranted using comprehensive and multimodal analysis.

Using an *in vitro* model system for neural differentiation using healthy and AD iPSC lines, we identified that LDN, ISO, and SAG greatly improved NG of AD iPSCs (Figures 3B–3F, S5B, 4A, and S2E). We also focused on the morphology of drug-treated neurons derived from AD iPSCs. Although the NG enhanced by these 3 drugs was so prominent that we could visually evaluate it, quantification of the morphology of the generated neurons also highlighted subtle differences in NG, enabling us to identify drug-dependent and cell-line-dependent effects. For example, the ratio of MAP2-to-TUJ1 area revealed that SAG generated a greater number of mature neurons from sAD3 than LDN and ISO, whereas this effect was not detected in sAD1 (Figure 3E). Additionally, these measures were used for PCA, after which clusters were generated following the cell line rather than the drug type (Figure 3F). Several studies have demonstrated the advantages of disease-specific human iPSC systems for revealing the characteristics of individual iPSCs (Kondo et al., 2017; Pasteuning-Vuhman et al., 2021). Thus, disease-specific iPSCs coupled with image-based quantification could support optimal drug selection to reverse neurogenetic inhibition in individual patients with AD for precision medicine.

On the basis of our results, we propose a molecular model for inhibiting NG in AD iPSCs (Figure 7I). First, SMAD1/5/9 is activated, which is initiated by an increase in BMP4

Figure 6. RUNX2 inhibition restored NG and oligodendrogenesis of sAD and fAD cells

(A) Quantitative real-time PCR analysis of *RUNX2* mRNA expression 0, 5, 10, 15, 20, 25, and 28 days after neuronal differentiation. The mean mRNA levels on day 0 of HC1 were set to 1. n = 4–6 independent experiments.

(B) The mRNA expression of *RUNX2* in cells treated with or without 250 nM LDN during stage II (left) and HC1–HC8 and sAD1–sAD8 iPSCs (right), analyzed by quantitative real-time PCR on day 28. The mean mRNA levels of HC1 were set to 1. n = 4–6 independent experiments. *p < 0.05.

(C) iPSCs from sAD and fAD patients were immunostained with MAP2 antibody (green) and TUJ1 antibody (yellow) after induction of neuronal differentiation with DMSO (0.5% [vol/vol], days 15–28) or CADD522 (50 μM, days 15–28, +CADD) for 28 days. Scale bar, 50 μm.

(D) Quantitative real-time PCR analysis of mRNA expression of *MAP2* and *TUJ1* under the same conditions as in (C). The mean mRNA levels in DMSO-treated sAD1 or fAD1 cells were set to 1. *p < 0.05 compared with DMSO-treated cells. n = 6 independent experiments.

(E) Immunofluorescence of OLIG2 and S100β under the same conditions as in (C).

(F) Immunofluorescence of cleaved caspase-3 (cCASP3) under the same conditions as in (C). Scale bar, 50 μm.

(G) Western blot of P-Smad1/5/9 and Runx2 in the hippocampus of 8-week SAMR1 or 8-week SAMP8 mice. n = 3 mice per group. The mean protein level of SAMR1 was set to 1. *p < 0.05.

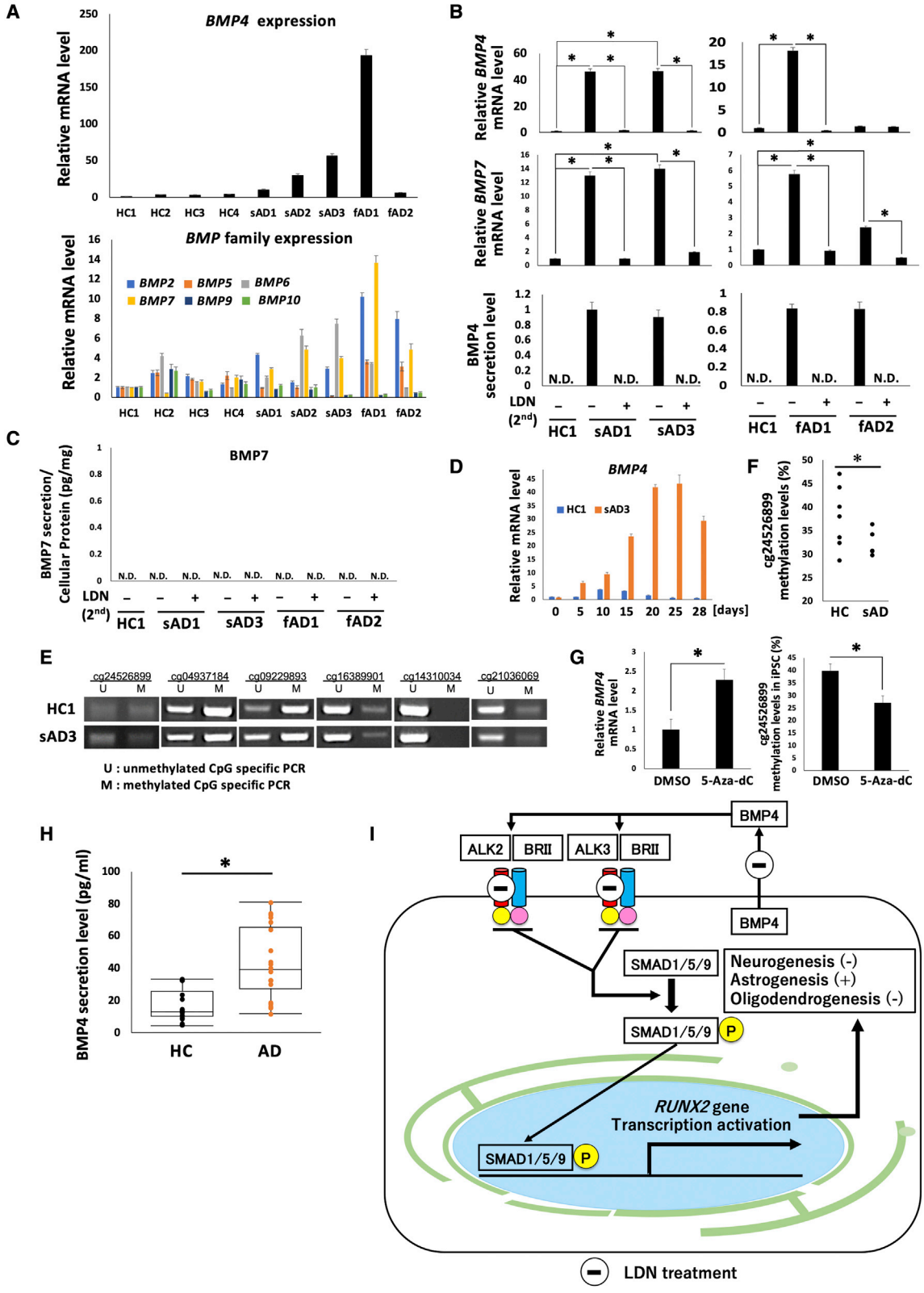

(legend on next page)

secretion. Then, the phosphorylated SMAD1/5/9 signal leads to elevated RUNX2-dependent transcription, subsequently inducing astrocyte differentiation as well as repressed generation of neurons and oligodendrocytes. This molecular model was validated *in vivo* using SAMP8 mice, which showed elevated Runx2 protein expression as well as enhanced phosphorylation of Smad1/5/9 (Figure 6G). Consistent with these findings and other reports (Li et al., 2008; Shou et al., 1999), secretion of BMP4 was enhanced in the cerebrospinal fluid of patients with AD (Figure 7H), suggesting that BMP4 hypersecretion might contribute to AD pathology. Interestingly, hypomethylation of cg24526899 of the *BMP4* promoter was commonly observed in AD iPSCs (Figures 7E and 7F). *BMP4* expression could form a positive feedback loop with phosphorylation of SMAD1/5/9 because LDN treatment decreased the expression level of BMP4 (Figure 7B). Furthermore, we found that inhibiting RUNX2 transcriptional activity with CADD522 restored NG and oligodendrocyte formation in AD iPSCs (Figure 6E). Previous reports have also suggested that the RUNX2 downstream target gene *SFRP2* enhances astrogenesis from NSCs through inhibition of NG and oligodendrogenesis (Chen and Mobley, 2019; Wen et al., 2020).

In this study, we report a novel *in vitro* model of deficient NG under cell senescence-related states in AD using patient-derived iPSCs and precise control of the culture environment. We also demonstrate that this *in vitro* model is a powerful tool for drug screening and for elucidating the molecular mechanisms underlying NG defects under senescence-related conditions in AD.

EXPERIMENTAL PROCEDURES

Resource availability

Corresponding author

Further information and requests for resources and reagents should be directed to the corresponding author, Fumi Kano (kano.f.aa@m.titech.ac.jp).

Materials availability

This study did not generate new unique reagents.

Data and code availability

Raw data and images are available upon request to the corresponding author.

iPSC culture

Healthy and sAD iPSC lines (HC1, HC2, HC4–HC8, and sAD1–sAD8) were a kind gift from Kyoto University through the Riken Cell Biology Center (Okita et al., 2011, 2013; Nakagawa et al., 2014; Kondo et al., 2013, 2017). The healthy iPSC line HC3 and the fAD iPSC lines (fAD1 and fAD2) were purchased from Takara Bio and the Coriell Institute, respectively. All iPSC lines were cultured on Matrigel (Corning, 356234)-coated 6-well plastic plates (Nunc, 140675) in mTeSR1 medium (STEMCELL Technologies, 85850).

SUPPLEMENTAL INFORMATION

Supplemental information can be found online at https://doi.org/10.1016/j.stemcr.2023.01.004.

AUTHOR CONTRIBUTIONS

D.N., M.M., and F.K. conceived and designed the experiments. D.N., R.K., Y.T., N.S.-N., K.O., K.Y., M.I., K.Hagiya, K.Hattori, T.T., and F.K. performed experiments. D.N., R.K., S.T., and S.Y. analyzed the data. D.N., R.K., Y.T., K.Hattori, and F.K. wrote the manuscript.

ACKNOWLEDGMENTS

We thank Prof. Haruhisa Inoue (Kyoto University) for providing the iPSC line and Prof. Akihiko Yoshimura (Keio University) for carefully reading and critically commenting on this manuscript. We also appreciate the Riken BioResource Center and the Center for iPS Cell Research and Application (CiRA) for kindly providing iPSC lines. We thank all volunteers who donated cerebrospinal fluid samples. Collection, storage, and distribution of human samples and associated data were supported by the NCNP Biobank, a member of National Center Biobank Network (NCBN). The NCNP Biobank is partly supported by a grant from the Japan Agency for Medical Research and Development (AMED), GAPFREE4 (21ak0101151h0002), and an Intramural Research Grant (3-1) for Neurological and Psychiatric Disorders of NCNP. Sample usage was

Figure 7. Elevated BMP4 level in AD cells and in cerebrospinal fluid samples from patients with AD

(A) After 28 days of neuronal differentiation, mRNA levels of *BMP2*, *BMP4*, *BMP5*, *BMP6*, *BMP7*, *BMP9*, and *BMP10* in control (HC1–HC4), sAD (sAD1–sAD3), and fAD (fAD1 and fAD2) cells were analyzed by quantitative real-time PCR. n = 4–6 independent experiments.

(B and C) mRNA expression and secretion of BMP4 and BMP7 on day 28. n = 6 independent experiments.

(D) Quantitative real-time PCR analysis of *BMP4* mRNA expression on days 0–28. n = 4 independent experiments. The mean mRNA levels of HC1 and sAD1 (A and B) and on day 0 of HC1 (C) were set to 1. *p < 0.05. N.D., not detected.

(E) Methylation levels of 6 CpG sites in the promoter region of the BMP4 gene were analyzed by unmethylated (U) and methylated (M) CpG-specific PCR in undifferentiated HC1 and sAD3 iPSCs.

(F) Methylation levels of cg245268999 of undifferentiated control (HC) and sAD iPSCs by EpiTaq HS. n = 5–7 independent experiments.

(G) mRNA expression of the *BMP4* gene and methylation levels of the CpG site (cg24526899) in the promoter region of control iPSCs (HC1) after treatment for 48 h with DMSO or 1 μM 5-aza-2′ deoxycytidine (5-Aza-dC). The mean mRNA levels of DMSO-treated HC1 were set to 1. n = 3 independent experiments.

(H) Concentrations of BMP4 in cerebrospinal fluid obtained from 20 HCs and 20 patients with AD.

(I) A model of NG inhibition in AD iPSCs. BRII, BMP receptor type 2.

supported by the AMED Biobank Network (AMED Platform Program for Promotion of Genome Medicine [JP21km0405401]). Furthermore, we thank Kenichi Ohba and Ryunosuke Tanemura (Nikon Systems Inc.) for assistance with analyzing neuron imaging and Shukun Hotta (Tokyo Institute of Technology) for experimental assistance. AMED-PRIME, AMED (JP21gm6210015) supported this work. This work was also supported by the FY2017 "Planting Seeds for Research" program from the Tokyo Institute of Technology.

CONFLICT OF INTERESTS

D.N., M.M., and F.K. have filed a patent related to this work.

Received: August 7, 2021
Revised: January 10, 2023
Accepted: January 10, 2023
Published: February 9, 2023

REFERENCES

Alzheimer's Association (2020). 2020 Alzheimer's disease facts and figures. Alzheimers Dement. *16*, 391–460.

Arber, C., Alatza, A., Leckey, C.A., Paterson, R.W., Zetterberg, H., and Wray, S. (2021). Mass spectrometry analysis of tau and amyloid-beta in iPSC-derived models of Alzheimer's disease and dementia. J. Neurochem. *159*, 305–317.

Attems, J., Walker, L., and Jellinger, K.A. (2014). Olfactory bulb involvement in neurodegenerative diseases. Acta Neuropathol. *127*, 459–475.

Boldrini, M., Fulmore, C.A., Tartt, A.N., Simeon, L.R., Pavlova, I., Poposka, V., Rosoklija, G.B., Stankov, A., Arango, V., Dwork, A.J., et al. (2018). Human hippocampal neurogenesis persists throughout aging. Cell Stem Cell *22*, 589–599.e5.

Chen, J.K., Taipale, J., Young, K.E., Maiti, T., and Beachy, P.A. (2002). Small molecule modulation of Smoothened activity. Proc. Natl. Acad. Sci. USA *99*, 14071–14076.

Chen, X.Q., and Mobley, W.C. (2019). Cachexia: a new definition. Clin. Nutr. *13*, 659.

Chen, X., Sun, G., Tian, E., Zhang, M., Davtyan, H., Beach, T.G., Reiman, E.M., Blurton-Jones, M., Holtzman, D.M., and Shi, Y. (2021). Modeling sporadic Alzheimer's disease in human brain organoids under serum exposure. Adv. Sci. *8*, e2101462.

Cline, E.N., Bicca, M.A., Viola, K.L., and Klein, W.L. (2018). The amyloid-β oligomer hypothesis: beginning of the third decade. J. Alzheimers Dis. *64*, S567–S610.

Clough, E., and Barrett, T. (2016). The gene expression omnibus database. Methods Mol. Biol. *1418*, 93–110.

Coupé, P., Manjón, J.V., Lanuza, E., and Catheline, G. (2019). Lifespan changes of the human brain in Alzheimer's disease. Sci. Rep. *9*, 3998.

Cummings, J., Lee, G., Ritter, A., Sabbagh, M., and Zhong, K. (2019). Alzheimer's disease drug development pipeline: 2019. Alzheimers Dement. *5*, 272–293.

Dan, X., Wechter, N., Gray, S., Mohanty, J.G., Croteau, D.L., and Bohr, V.A. (2021). Olfactory dysfunction in aging and neurodegenerative diseases. Ageing Res. Rev. *70*, 101416.

Dard, R.F., Dahan, L., and Rampon, C. (2019). Targeting hippocampal adult neurogenesis using transcription factors to reduce Alzheimer's disease-associated memory impairments. Hippocampus *29*, 579–586.

Díaz-Moreno, M., Armenteros, T., Gradari, S., Hortigüela, R., García-Corzo, L., Fontán-Lozano, Á., Trejo, J.L., and Mira, H. (2018). Noggin rescues age-related stem cell loss in the brain of senescent mice with neurodegenerative pathology. Proc. Natl. Acad. Sci. USA *115*, 11625–11630.

Drummond, E., and Wisniewski, T. (2017). Alzheimer's disease: experimental models and reality. Acta Neuropathol. *133*, 155–175.

Elkabetz, Y., Panagiotakos, G., Al Shamy, G., Socci, N.D., Tabar, V., and Studer, L. (2008). Human ES cell-derived neural rosettes reveal a functionally distinct early neural stem cell stage. Genes Dev. *22*, 152–165.

Fricker, M., Tolkovsky, A.M., Borutaite, V., Coleman, M., and Brown, G.C. (2018). Neuronal cell death. Physiol. Rev. *98*, 813–880.

He, N., Jin, W.L., Lok, K.H., Wang, Y., Yin, M., and Wang, Z.J. (2013). Amyloid-β(1-42) oligomer accelerates senescence in adult hippocampal neural stem/progenitor cells via formylpeptide receptor 2. Cell Death Dis. *4*, e924.

Hollands, C., Tobin, M.K., Hsu, M., Musaraca, K., Yu, T.-S., Mishra, R., Kernie, S.G., and Lazarov, O. (2017). Depletion of adult neurogenesis exacerbates cognitive deficits in Alzheimer's disease by compromising hippocampal inhibition. Mol. Neurodegener. *12*, 64.

Kondo, T., Asai, M., Tsukita, K., Kutoku, Y., Ohsawa, Y., Sunada, Y., Imamura, K., Egawa, N., Yahata, N., Okita, K., et al. (2013). Modeling Alzheimer's disease with iPSCs reveals stress phenotypes associated with intracellular Aβ and differential drug responsiveness. Cell Stem Cell *12*, 487–496.

Kondo, T., Imamura, K., Funayama, M., Tsukita, K., Miyake, M., Ohta, A., Woltjen, K., Nakagawa, M., Asada, T., Arai, T., et al. (2017). iPSC-based compound screening and in vitro trials identify a synergistic anti-amyloid β combination for Alzheimer's disease. Cell Rep. *21*, 2304–2312.

Kondo, T., Hara, N., Koyama, S., Yada, Y., Tsukita, K., Nagahashi, A., Ikeuchi, N., Ishii, K., Asada, T., Arai, T., et al. (2022). Dissection of the polygenic architecture of neuronal Aβ production using a large sample of individual iPSC lines derived from Alzheimer's disease patients. Nature Aging *2*, 125–139.

Lampinen, R., Fazaludeen, M.F., Avesani, S., Örd, T., Penttilä, E., Lehtola, J.M., Saari, T., Hannonen, S., Saveleva, L., Kaartinen, E., et al. (2022). Single-cell RNA-seq analysis of olfactory mucosal cells of alzheimer's disease patients. Cells *11*, 676.

Lane, M.A., and Bailey, S.J. (2005). Role of retinoid signalling in the adult brain. Prog. Neurobiol. *75*, 275–293.

Li, D., Tang, J., Xu, H., Fan, X., Bai, Y., and Yang, L. (2008). Decreased hippocampal cell proliferation correlates with increased expression of BMP4 in the APPswe/PS1DeltaE9 mouse model of Alzheimer's disease. Hippocampus *18*, 692–698.

Li Puma, D.D., Piacentini, R., Leone, L., Gironi, K., Marcocci, M.E., De Chiara, G., Palamara, A.T., and Grassi, C. (2019). Herpes

simplex virus type-1 infection impairs adult hippocampal neurogenesis via amyloid-β protein accumulation. Stem Cell. *37*, 1467–1480.

Malek-Ahmadi, M., Chen, K., Perez, S.E., He, A., and Mufson, E.J. (2018). Cognitive composite score association with Alzheimer's disease plaque and tangle pathology. Alzheimer's Res. Ther. *10*, 90.

Moreno-Jiménez, E.P., Flor-García, M., Terreros-Roncal, J., Rábano, A., Cafini, F., Pallas-Bazarra, N., Ávila, J., and Llorens-Martín, M. (2019). Adult hippocampal neurogenesis is abundant in neurologically healthy subjects and drops sharply in patients with Alzheimer's disease. Nat. Med. *25*, 554–560.

Nakagawa, M., Taniguchi, Y., Senda, S., Takizawa, N., Ichisaka, T., Asano, K., Morizane, A., Doi, D., Takahashi, J., Nishizawa, M., et al. (2014). A novel efficient feeder-free culture system for the derivation of human induced pluripotent stem cells. Sci. Rep. *4*, 3594.

Nicaise, A.M., Willis, C.M., Crocker, S.J., and Pluchino, S. (2020). Stem cells of the aging brain. Front. Aging Neurosci. *12*, 247.

Okawa, S., Nicklas, S., Zickenrott, S., Schwamborn, J.C., and Del Sol, A. (2016). A generalized gene-regulatory Network model of stem cell differentiation for predicting lineage specifiers. Stem Cell Rep. *7*, 307–315.

Okita, K., Matsumura, Y., Sato, Y., Okada, A., Morizane, A., Okamoto, S., Hong, H., Nakagawa, M., Tanabe, K., Tezuka, K.i., et al. (2011). A more efficient method to generate integration-free human iPS cells. Nat. Methods *8*, 409–412.

Okita, K., Yamakawa, T., Matsumura, Y., Sato, Y., Amano, N., Watanabe, A., Goshima, N., and Yamanaka, S. (2013). An efficient nonviral method to generate integration-free human-induced pluripotent stem cells from cord blood and peripheral blood cells. Stem Cell. *31*, 458–466.

Ortiz-Montero, P., Londoño-Vallejo, A., and Vernot, J.P. (2017). Senescence-associated IL-6 and IL-8 cytokines induce a self- and cross-reinforced senescence/inflammatory milieu strengthening tumorigenic capabilities in the MCF-7 breast cancer cell line. Cell Commun. Signal. *15*, 17.

Pasteuning-Vuhman, S., de Jongh, R., Timmers, A., and Pasterkamp, R.J. (2021). Towards advanced iPSC-based drug development for neurodegenerative disease. Trends Mol. Med. *27*, 263–279.

Rajmohan, R., and Reddy, P.H. (2017). Amyloid-beta and phosphorylated tau accumulations cause abnormalities at synapses of Alzheimer's disease neurones. J. Alzheimers Dis. *57*, 975–999.

Ray, S., Corenblum, M.J., Anandhan, A., Reed, A., Ortiz, F.O., Zhang, D.D., Barnes, C.A., and Madhavan, L. (2018). A role for Nrf2 expression in defining the aging of hippocampal neural stem cells. Cell Transplant. *27*, 589–606.

Richetin, K., Leclerc, C., Toni, N., Gallopin, T., Pech, S., Roybon, L., and Rampon, C. (2015). Genetic manipulation of adult-born hippocampal neurones rescues memory in a mouse model of Alzheimer's disease. Brain *138*, 440–455.

Sanchez-Duffhues, G., Williams, E., Goumans, M.J., Heldin, C.,H., and Ten Dijke, P. (2020). Bone morphogenetic protein receptors: structure, function and targeting by selective small molecule kinase inhibitors. Bone *138*, 115472.

Schulz, J.M. (2021). The potential of induced pluripotent stem cells to treat and model Alzheimer's disease. Stem Cells Int. *2021*, 5511630.

Scopa, C., Marrocco, F., Latina, V., Ruggeri, F., Corvaglia, V., La Regina, F., Ammassari-Teule, M., Middei, S., Amadoro, G., Meli, G., et al. (2020). Impaired adult neurogenesis is an early event in Alzheimer's disease neurodegeneration, mediated by intracellular Abeta oligomers. Cell Death Differ. *27*, 934–948.

Shou, J., Rim, P.C., and Calof, A.L. (1999). BMPs inhibit neurogenesis by a mechanism involving degradation of a transcription factor. Nat. Neurosci. *2*, 339–345.

Storer, M.A., Gallagher, D., Fatt, M.P., Simonetta, J.V., Kaplan, D.R., and Miller, F.D. (2018). Interleukin-6 regulates adult neural stem cell numbers during normal and abnormal post-natal development. Stem Cell Rep. *10*, 1464–1480.

Tang, J., Song, M., Wang, Y., Fan, X., Xu, H., and Bai, Y. (2009). Noggin and BMP4 co-modulate adult hippocampal neurogenesis in the APP(swe)/PS1(DeltaE9) transgenic mouse model of Alzheimer's disease. Biochem. Biophys. Res. Commun. *385*, 345–351.

Tiwari, N., Pataskar, A., Péron, S., Thakurela, S., Sahu, S.K., Figueres-Oñate, M., Marichal, N., López-Mascaraque, L., Tiwari, V.K., and Berninger, B. (2018). Stage-specific transcription factors drive astrogliogenesis by remodeling gene regulatory landscapes. Cell Stem Cell *23*, 557–571.e8.

Tobin, M.K., Musaraca, K., Disouky, A., Shetti, A., Bheri, A., Honer, W.G., Kim, N., Dawe, R.J., Bennett, D.A., Arfanakis, K., et al. (2019). Human hippocampal neurogenesis persists in aged adults and Alzheimer's disease patients. Cell Stem Cell *24*, 974–982.e3.

Toda, T., Parylak, S.L., Linker, S.B., and Gage, F.H. (2019). The role of adult hippocampal neurogenesis in brain health and disease. Mol. Psychiatry *24*, 67–87.

Vyas, Y., Montgomery, J.M., and Cheyne, J.E. (2020). Hippocampal deficits in amyloid-β-related rodent models of Alzheimer's disease. Front. Neurosci. *14*, 266.

Wattanapanitch, M., Klincumhom, N., Potirat, P., Amornpisutt, R., Lorthongpanich, C., U-pratya, Y., Laowtammathron, C., Kheolamai, P., Poungvarin, N., and Issaragrisil, S. (2014). Dual small-molecule targeting of SMAD signaling stimulates human induced pluripotent stem cells toward neural lineages. PLoS One *9*, e106952.

Wen, Q., Jing, J., Han, X., Feng, J., Yuan, Y., Ma, Y., Chen, S., Ho, T.-V., and Chai, Y. (2020). Runx2 regulates mouse tooth root development via activation of WNT inhibitor NOTUM. J. Bone Miner. Res. *35*, 2252–2264.

Wheatley, E.G., Albarran, E., White, C.W., 3rd, Bieri, G., Sanchez-Diaz, C., Pratt, K., Snethlage, C.E., Ding, J.B., and Villeda, S.A. (2019). Neuronal O-GlcNAcylation improves cognitive function in the aged mouse brain. Curr. Biol. *29*, 3359–3369.e4.

Wirths, O. (2017). Altered neurogenesis in mouse models of Alzheimer disease. Neurogenesis (Austin) *4*, e1327002.

Yu, P.B., Deng, D.Y., Lai, C.S., Hong, C.C., Cuny, G.D., Bouxsein, M.L., Hong, D.W., McManus, P.M., Katagiri, T., Sachidanandan, C., et al. (2008). BMP type I receptor inhibition reduces heterotopic ossification. Nat. Med. *14*, 1363–1369.

Zhang, S.C., Wernig, M., Duncan, I.D., Brüstle, O., and Thomson, J.A. (2001). In vitro differentiation of transplantable neural precursors from human embryonic stem cells. Nat. Biotechnol. *19*, 1129–1133.

Zhang, Z.H., Chen, C., Wu, Q.Y., Zheng, R., Chen, Y., Liu, Q., Ni, J.Z., and Song, G.L. (2016). Selenomethionine ameliorates neuropathology in the olfactory bulb of a triple transgenic mouse model of Alzheimer's disease. Int. J. Mol. Sci. *17*, 1595.